PHYSICAL REVIEW B

CONDENSED MATTER

THIRD SERIES, VOLUME 48, NUMBER 4 15 JULY 1993-II

Electron-phonon interactions and the phonon anomaly in β-phase NiTi

G. L. Zhao and B. N. Harmon

Ames Laboratory and Department of Physics and Astronomy, Iowa State University, Ames, Iowa 50010

(Received 11 January 1993)

The electronic structure of β-phase NiTi has been calculated using a first-principles linear-combination-of-atomic-orbitals method. The resulting band structure was fitted with a nonorthogonal tight-binding Hamiltonian from which electron-phonon matrix elements were evaluated. The soft phonon near $Q_0=(\frac{2}{3},\frac{2}{3},0)\pi/a$, which is responsible for the premartensitic phase transition in β-phase NiTi, is found to arise from the strong electron-phonon coupling of nested electronic states on the Fermi surface. Thermal vibrations and changes in electronic occupation cause a smearing of the nested features, which in turn cause a hardening of the phonon anomaly.

I. INTRODUCTION

Equiatomic NiTi is perhaps the best known and technologically the most important compound exhibiting the shape-memory effect, which is related to a reversible martensitic transformation.[1-3] At high temperatures, NiTi possesses a simple cubic CsCl-type structure (also called the $B2$ or β-phase structure). As temperature is lowered, β-phase NiTi undergoes a displacive structural transformation to an intermediate or so-called R phase at about 293 K, and then undergoes a martensitic transformation to a monoclinic structure near 273 K.[4-7] The exact temperature of the phase transformation depends on stoichiometry. X-ray and electron-diffraction studies have revealed superlattice spots associated with the R phase.[8,9] In addition, inelastic neutron-scattering experiments have found that the TA_2 [110] (or Σ_4) phonon branch in the β phase is temperature dependent and becomes soft near $\mathbf{Q}_0=\frac{1}{3}(1,1,0)2\pi/a$ at about room temperature.[10-15] The condensation of this soft phonon mode is responsible for the premartensitic or R-phase structure. This phase transformation can account for the most prominent premartensitic phenomena, such as the $\frac{1}{3}$-type superstructure reflections, the internal friction, and the electrical resistivity anomalies.[16-19] A model for the R transformation was proposed by Shapiro *et al.*,[8] and extended by Folkins and Walker, who presented a fairly complete Landau expansion of the free energy which included the coupling of phonon displacements and lattice strains.[20] The origin of the phonon softening at Q_0 has long been speculated to be due to Fermi surface nesting;[12,21] however, a previous calculation of the phonon-dispersion curves in β-phase NiTi which included an evaluation of approximate electron-phonon (e-ph) matrix elements failed to show any feature near $\mathbf{Q}_0$ which would explain the sharp phonon anomaly found in the measurements.[22] Questions have therefore been raised about other possible driving mechanisms for the anomalies.[23]

It is the purpose of this paper to give details of a calculation of the phonon-dispersion curves of NiTi which include more accurate electron-phonon matrix elements and which clearly demonstrate the electronic origin of the observed phonon anomaly. We briefly reported on this work in a previous publication,[24] and here we review the important results, supply details, and include "temperature-dependent" phonon-dispersion curves which highlight the sharpness of the Fermi surface nesting. A slightly better set of empirical parameters was found for the band structure and short-range force constants, and these are also presented.

II. ELECTRONIC STRUCTURE

A study of the e-ph interaction requires the calculation of the electronic structure and the evaluation of e-ph matrix elements. As the first step, the electronic structure of β-phase equiatomic NiTi was calculated using a self-consistent first-principles linear-combination-of-atomic-orbitals (LCAO) method.[25] The density of states from the first-principles calculation is given in Fig. 1. The peaks in the density of states at low energy (from about -0.3 to -0.1 Ry) are mainly from Ni $3d$ states, while the peaks around E_F (here $E_F=0$) are mainly from Ti $3d$ states.

The first-principles band structure was fitted using a nonorthogonal Slater-Koster tight-binding Hamiltonian.[26] A high-quality fit of the bands is vital for the calculation of the e-ph interaction since a subtle distortion of the Fermi surface may smear out any nesting feature contributing to the phonon anomaly. Thus special attention is needed in the fitting procedure. In this calculation 15

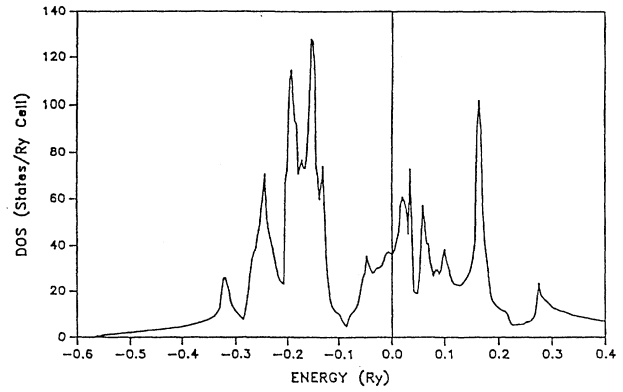

FIG. 1. The total density of states for β-phase NiTi from the first-principles calculation. The Fermi energy (E_F) has been set as zero. The low-energy peaks are mainly from the d states of Ni, and the peaks around the Fermi energy are mainly from the d states of Ti.

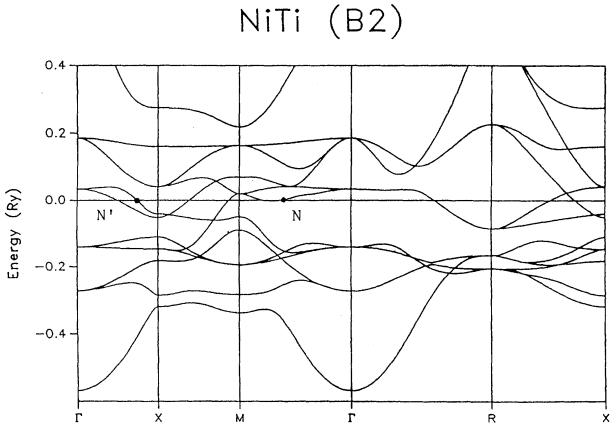

FIG. 2. Electronic energy bands of β-phase NiTi. The bands were calculated by using a first-principles LCAO method and then fitted by an empirical tight-binding Hamiltonian.

k points were used, which were chosen at the high-symmetry points or lines in the irreducible Brillouin zone. At the first stage of the fitting, all the bands of the 15 high-symmetry k points were used and an average rms error of about 2.7 m Ry was reached. Group theory was used to fit the irreducible representations separately. Then the energy bands around the Fermi energy ($E_F=0$) were assigned higher weight since these bands are the most important for the e-ph interaction. An average rms error of 1.8 m Ry was obtained, with the fitting errors for the energy bands around E_F being about 1 m Ry. The fitted tight-binding (TB) parameters are listed in Table I.

TABLE I. The TB parameters for β-phase NiTi (in Ry). E_s, E_p, and E_d are the atomic energy levels; c.f. (1st) and c.f. (2nd) are the empirical crystal-field parameters for the first and second shell of atoms; H stands for Hamiltonian and S for overlap.

Atom	E_s	E_p	E_d	c.f. (1st)	c.f. (2nd)
Ni	0.3268	0.6816	−0.1247	0.0034	−0.0040
Ti	0.2063	0.6114	0.0442	0.0109	0.0052
Pair	$ss\sigma$	$sp\sigma$	$sd\sigma$	$pp\sigma$	$pp\pi$
	$pd\sigma$	$pd\pi$	$dd\sigma$	$dd\pi$	$dd\delta$
			H		
Ni-Ni	−0.0007	0.0451	−0.0111	0.0930	0.0046
	−0.0313	−0.0088	−0.0172	0.0052	−0.0003
Ni-Ti	−0.1324	0.1405	−0.0576	0.1194	−0.0247
	−0.0754	0.0332	−0.0495	0.0311	−0.0031
Ti-Ti	−0.0519	0.0706	−0.0478	0.1282	−0.0285
	−0.0620	0.0391	−0.0413	0.0268	−0.0032
			S:		
Ni-Ni	0.0467	−0.0331	−0.0900	−0.0753	0.0173
	−0.0606	−0.0197	0.0092	−0.0391	−0.0071
Ni-Ti	0.0399	−0.0792	0.0034	−0.1378	0.0453
	−0.0041	−0.0559	0.0100	−0.0156	0.0114
Ti-Ti	0.0793	−0.1104	0.0605	−0.1381	0.0381
	0.0489	−0.0098	0.0556	0.0351	−0.0070

In the case of β-phase NiTi, only bands 7 and 8 (from the bottom) cross the Fermi energy, and give the dominant e-ph interaction contributions to the phonon dynamical matrix. As a whole, the TB fitted band structure is indistinguishable from that obtained from the first-principles calculation. In Fig. 2, the TB band structure has been drawn along some of the high-symmetry directions, and the Fermi energy E_F has been chosen to be zero. The band structure in Fig. 2 looks similar to that of Papaconstantopoulos, Kamm, and Poulopoulos,[21] which was the band structure used in an earlier evaluation of the e-ph interaction.[22] As we pointed out below, there are subtle differences in the Fermi surfaces of the two calculations which occur near the nesting region. In addition, the simplification used by Bruinsma[22] for the e-ph matrix elements results in an incorrect weak coupling to the TA_2 phonon branch. The relevant nesting feature of the Fermi surface is displayed in Fig. 3, with the spanning vector $Q_0=(\frac{2}{3},\frac{2}{3},0)\pi/a$ shown. The nested Fermi surface region of band 7 is near the Γ-M line and is labeled N in Fig. 2, while the band-8 nested region is near the Γ-X line and is labeled N' in Fig. 2. The Fermi energy E_F is very

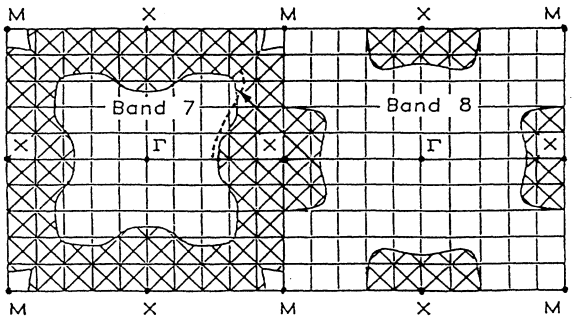

FIG. 3. The Fermi surface of band 7 in the left zone and band 8 in the right zone. The shaded areas are occupied. The arrow shows the wave vector Q_0 between the nested regions. The dashed curve shows a piece of the NiTi Fermi surface from the calculation of Ref. 21.

close to the bottom of band 7 near the N point. A small shift of E_F or of the band structure (e.g., by alloying) will move the position of the nesting away from $Q_0=(\frac{2}{3},\frac{2}{3},0)\pi/a$.

III. CALCULATION OF THE PHONON ANOMALY

A. Method and formulas

The contribution of the e-ph interaction to the phonon dynamical matrix can be evaluated by second-order perturbation theory. We follow the method of Varma and Weber.[27] The total dynamical matrix can be divided into a short-range part (denoted as D_0+D_1 in Ref. 27) and a long-range part D_2, which is responsible for the sharp features in the phonon-dispersion curves. The short-range part of the dynamical matrix can be modeled with a few Born–von Kármán force constants (listed in Table II) which we obtained by fitting the theoretical dispersion curves to the measured phonon frequencies at high-symmetry points. The phonon-dispersion curves from only the short-range Born–von Kármán model are smooth and featureless. They are shown in Fig. 3 of Ref. 24. The important e-ph interactions arise from the D_2 part of the dynamical matrix, which is given by

$$D_2(\kappa\alpha,\kappa'\alpha'|\mathbf{q})=-\sum_{\mathbf{k}\mu\nu}\frac{f_{\mathbf{k}\mu}(1-f_{\mathbf{k}+\mathbf{q}\nu})}{\varepsilon_{\mathbf{k}+\mathbf{q}\nu}-\varepsilon_{\mathbf{k}\mu}}\times g^{\kappa\alpha}_{\mathbf{k}\mu,\mathbf{k}+\mathbf{q}\nu}g^{\kappa'\alpha'}_{\mathbf{k}+\mathbf{q}\nu,\mathbf{k}\mu}\ , \tag{1}$$

in which

$$g^{\kappa\alpha}_{\mathbf{k}\mu,\mathbf{k}'\nu}=\sum_{\beta_1 m_1\beta_2 m_2}A^*(\mathbf{k}'\nu|\beta_1 m_1)\times[\gamma_\alpha(\beta_1 m_1\beta_2 m_2|\mathbf{k})\delta_{\beta_1\kappa}-\gamma_\alpha(\beta_1 m_1\beta_2 m_2|\mathbf{k}')\delta_{\beta_2\kappa}]\times A(\mathbf{k}\mu|\beta_2 m_2) \tag{2}$$

and

$$\gamma_\alpha(\beta_1 m_1\beta_2 m_2|\mathbf{k})=\sum_l\left\langle\phi_{\beta_1 m_1}\left|\frac{\partial H}{\partial u_\alpha(\beta_1 l_1,\beta_2 l_2)}\right|\phi_{\beta_2 m_2}\right\rangle\times e^{-i\mathbf{k}\cdot\mathbf{R}(\beta_1 l_1,\beta_2 l_2)}\ . \tag{3}$$

Here $|\phi_{\beta m}\rangle$ is the mth orbital of the atomic wave function at site β; $\mathbf{R}(l_1\beta_1,l_2\beta_2)=\mathbf{R}(l_1\beta_1)-\mathbf{R}(l_2\beta_2)$; $A(\mathbf{k}\mu|\beta m)$ is the (βm) component of μth eigenstate at the wave vector $\mathbf{k}$; $\varepsilon_{\mathbf{k}\mu}$ is the energy of the μth band at $\mathbf{k}$; H is the Hamiltonian; $u_\alpha(\beta l)$ is the displacement of the atom at site β of the lth cell; and $f_{\mathbf{k}\mu}$ is the Fermi distribution function which gives the temperature dependence of electron occupation.

TABLE II. The longitudinal (l) and transverse (t) short-range axially symmetric force constants for (D_0+D_1) used in the Born–von Kármán model for the β-phase of Ni-Ti.

Pair	Shell	r (Å)	(l) (10^3 dyn/cm)	(t) (10^3 dyn/cm)
Ni-Ni	1st	3.015	−0.3835	−2.5697
Ni-Al	1st	2.611	40.9651	−3.5358
Al-Al	1st	3.015	56.0682	−4.5049

In the summation over bands in Eq. (1), we included only bands 7 and 8, which cross the Fermi level. The other band contributions are generally featureless and have been lumped together with the D_0+D_1 short-range contributions to the dynamical matrix.

For the k-space summation, the Brillouin zone was partitioned into cubes on a $\pi/20a$ mesh and the e-ph matrix elements were assumed to be constant within each cube. The tetrahedron method was used to perform the analytic integration for the linearly interpolated energy bands within each cube.[28]

B. Phonon anomaly

The calculated low-temperature phonon-dispersion curves for the acoustic modes along three high-symmetry directions are shown as the solid lines in Figs. 4(a), 4(b), and 4(c). The symbols shown in these figures are the experimental data points.[29] The dip in the lowest transverse-acoustic [110] branch actually goes soft (i.e., the dynamical matrix yields an imaginary frequency) at $Q_0=(0.65,0.65,0)\pi/a$. Because the calculated phonons are restricted to the $\pi/20a$ mesh, it is possible that the minimum in the dip occurs slightly away from this value of Q_0. A calculation on a much finer mesh of just the bare susceptibility, $\chi(\mathbf{q})$, which is the same as Eq. (1) but without the e-ph matrix elements, suggests that the minimum of the dip should be closer to $Q_0=(0.64,0.64,0)\pi/a$.[24]

The experiments indicate that the phonon dip in the [110] TA_2 branch goes soft near 293 K and has a very dramatic temperature dependence.[13] While a theoretical treatment of all temperature-dependent effects is very difficult, it is possible to study how smearing the Fermi surface can reduce the nesting and influence the phonon dip. The smearing of the Fermi surface arises from disorder caused by thermal vibrations or by temperature-independent disorder from impurities, defects, nonstoichiometry, antiphase boundaries, etc. Even without these sources of disorder, the Fermi surface would be smeared at higher temperatures by changes in the electronic Fermi-Dirac occupations. It is very simple to introduce temperature as a parameter in the Fermi function, and evaluate Eq. (1) with various degrees of Fermi-surface smearing. The phonon-dispersion curves obtained for "temperatures" of 320, 500, and 1000 K are also shown in Figs. 4(a), 4(b), and 4(c). The short-range force constants were kept the same (Table II), so only changes in D_2 arising from changes in the Fermi-Dirac occupation account for the changes in the dispersion curves.

Figure 4(a) shows that just a small amount of smearing the Fermi surface is enough to stabilize the Q_0 phonon mode, and that with an effective temperature of only 1000 K ($kT\approx 0.1$ eV) the phonon anomaly has nearly

disappeared. Experimentally, the anomaly is weakened at somewhat lower temperatures,[13] because of the other thermal contributions to the smearing. Figure 4(a) also shows that, because the longitudinal branch is coupled to the same set of electronic states, it also has a noticeable "temperature" dependence in the region of Q_0. The e-ph symmetries which cause strong coupling to the [110] LA and TA_2 branches, but not the TA_1, branch, are discussed in the next section.

We note that there is also some sensitivity to "temperature" exhibited by the longitudinal [111] phonon branch, but there are not specific q vectors where nesting occurs. Rather, there are many states near E_F which contribute over a wide range of q values. It is also this region that gave the poorest agreement with experiment, so that those states near E_F giving rise to the larger electronic screening and lower theoretical phonon frequencies may not be accurately positioned. The dispersion curves along the [100] direction show little "temperature" dependence. The theoretical curve for the longitudinal branch in this direction exhibits wiggles which we believe are caused by numerical noise and the fact that we evaluated the frequencies on a finite mesh (every 0.05 units).

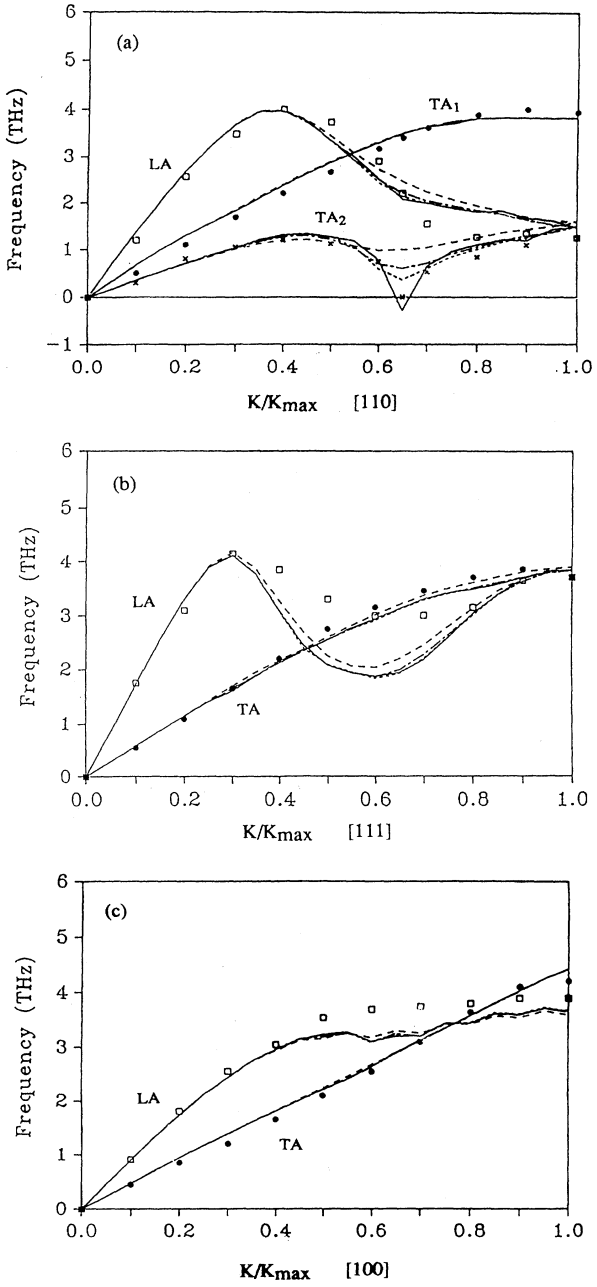

FIG. 4. The phonon-dispersion curves of β-phase NiTi. All the symbols are the experimental results (Ref. 29). The squares are the longitudinal phonons and the dots and crosses are the transverse-acoustic phonons. The lines are the calculated results. ——, $T=1$ K; · · · ·, 320 K; —·—·—·, 500 K; and — — —, 1000 K. The acoustic phonons are along (a) the [110], (b) the [111], and (c) the [110] directions.

C. Analysis of the D_2 matrix at $\mathbf{q}\simeq(0.65,0.65,0)\pi/a$

The soft phonon of the TA_2 branch with a polarization along $\langle 1\bar{1}0\rangle$ at $\mathbf{q}\simeq(0.65,0.65,0)\pi/a$ is caused by the strong coupling of the electronic states at the Fermi surface. The most important contribution to $D_2(\mathbf{q})$ at $\mathbf{q}\simeq(0.65,0.65,0)\pi/a$ comes from the coupling of electronic states ($\mathbf{k}$ and $\mathbf{k}+\mathbf{q}$) across the nesting feature of the Fermi surface, as in Fig. 3. From the analysis of the wave functions of states in these regions, we find that the dominant contribution is from the coupling between states at $\mathbf{k}$ with Ti $d_{x^2-y^2}$ character and states at $\mathbf{k}+\mathbf{q}$ with Ni d_{xy} character. A schematic representation for these orbitals is shown in Fig. 5. The overlap matrix between these two states is zero when the Ni and Ti atoms are at rest on the regular lattice, that is,

$$\langle d^{(\mathrm{Ti})}_{x^2-y^2}|d^{(\mathrm{Ni})}_{xy}\rangle=0.0\ ,$$

where the x^2-y^2 character of Ti comes from states with wave vector $\mathbf{k}$ on one piece of the Fermi surfaces and the xy character of Ni from states at $(\mathbf{k}+\mathbf{q})$ on the other side. Here $\mathbf{q}\simeq(0.65,0.65,0)\pi/a$. Because of the symme-

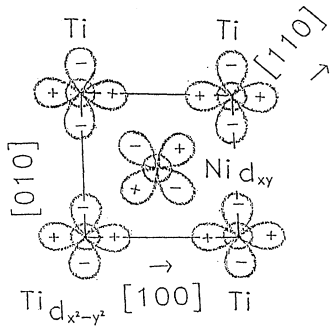

FIG. 5. A depiction of the coupling of the wave functions with Ti $d_{x^2-y^2}$ and Ni d_{xy} characters, which make the most important contributions to the electron-phonon matrix elements causing the soft phonon in the TA_2 branch along the [110] direction. Note that the Ni orbital is not in the same plane as the Ti orbitals.

try properties of the Ti $d_{x^2-y^2}$ and the Ni d_{xy} wave functions, these two states have zero overlap (see Fig. 5). The vibrations of atoms change the situation. The vibration of atoms along the $\langle 1\bar{1}0\rangle$ direction, which is the polarization of the TA_2 [110] phonon, will destroy the symmetry. Such a situation can give rise to large e-ph matrix elements which are proportional to the gradient of the overlap or Hamiltonian matrix elements. The vibration of atoms along the $\langle 110\rangle$ direction, which is the polarization direction of the longitudinal [110] phonon (LA), will have almost the same effect. So the $D_2(\mathbf{q})$ matrix in this region receives a large contribution from atomic vibrations along the $\langle 1\bar{1}0\rangle$ and $\langle 110\rangle$ directions, which correspond to the TA_2 and LA phonon branches. However, the movements of atoms along the $\langle 001\rangle$ direction do not have this effect and make little contribution to the $D_2(\mathbf{q})$ matrix. The longitudinal phonon has a much higher phonon frequency at $\mathbf{q}\simeq(0.65,0.65,0)\pi/a$ than that of the TA_2 transverse phonon, so the coupling of electronic states from the nesting feature of the Fermi surface can drive the TA_2 phonon soft, but will only lower the frequency of the LA phonon, as in Fig. 4(a). This is made clear by considering the differences of phonon frequencies between the two calculations, one of which includes D_2 and another without D_2. If we define

$$\Delta f = f(\text{no } D_2) - f(\text{with } D_2) ,$$

where f is the phonon frequency, we find

$$TA_2:\ \Delta f(\langle 1\bar{1}0\rangle) = 3.29 \text{ (THz)} ,$$

$$LA:\ \Delta f(\langle 110\rangle) = 2.72 \text{ (THz)} ,$$

$$TA_1:\ \Delta f(\langle 001\rangle) = 0.38 \text{ (THz)} ,$$

at $\mathbf{q}=(0.65,0.65,0)\pi/a$.[30] The difference between the D_2 contributions for the LA and TA_2 modes arises from the other orbital components of the electronic wave functions in the nesting regions. The shift in frequency for the TA_1 mode also arises from these other symmetry components and is small.

D. β-phase Ni_xTi_{1-x} alloys

For β-phase Ni_xTi_{1-x}, alloys, where x is close 0.5, the rigid-band model may be a reasonable description for some of the properties of the system. We can then use the same electronic band structure for all the β-phase Ni_xTi_{1-x} alloys, but the Fermi energies will be different for different concentrations according to the total number of valence electrons. Since the position of the phonon anomaly and the strength of the e-ph coupling are sensitive to the Fermi energy, a slight shift of the Fermi energy results in a noticeable change in the position of the phonon anomaly. It can also affect the transition temperature at which the phonon becomes soft, as in the case of β-phase Ni_xAl_{1-x} alloys. By using the rigid-band model, the position of the phonon anomaly of β-phase Ni_xTi_{1-x} alloys has been examined. With a $\pi/20a$ mesh, it is difficult to follow theoretically subtle changes in the phonon-dispersion curves; however, if the e-ph matrix elements are reasonably constant over the k-space region of interest, we can easily evaluate the generalized susceptibility $\chi(\mathbf{q})$ and follow the peak position as a function of the electron count.

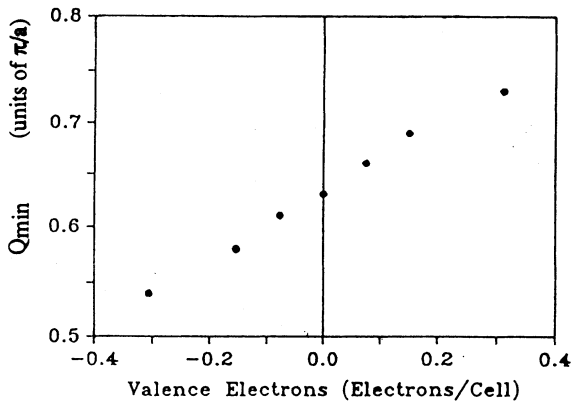

FIG. 6. The calculated positions of the phonon anomaly, $Q_{\min}$, along the [110] direction as the function of the number of valence electrons. (The 0 corresponds to β-phase $Ni_{0.50}Ti_{0.50}$.)

The generalized susceptibility $\chi(\mathbf{q})$ is defined as[28]

$$\chi(\mathbf{q}) = \sum_{\mathbf{k}\mu\nu} \frac{f_{\mathbf{k}\mu}(1-f_{\mathbf{k}+\mathbf{q}\nu})}{\varepsilon_{\mathbf{k}+\mathbf{q}\nu}-\varepsilon_{\mathbf{k}\mu}} , \tag{4}$$

which differs from the formula of $D_2(\mathbf{q})$ only by the multiplication of the e-ph coupling matrix elements. If we take all the e-ph coupling matrix elements to be constant, then the formula of $D_2(\mathbf{q})$ reduces to the formula of $\chi(\mathbf{q})$. By shifting the Fermi energy and using the same band structure, the peak in $\chi(\mathbf{q})$ has been calculated, and is given in Fig. 6 as a function of the total number of valence electrons. It can be seen that a small shift of Fermi energy can have a dramatic effect on the position of the phonon anomaly. A downward shift of Fermi energy by 0.006 Ry (about -0.35 electrons/cell), and the peak position of $\chi(\mathbf{q})$ is moved from about $Q_0=(0.63,0.63,0)\pi/a$ to $Q_0=(0.58,0.58,0)\pi/a$.

IV. CONCLUSION

From our study, it is found that an accurate calculation of e-ph interaction can explain the behavior of the phonon anomaly in β-phase NiTi alloys. The soft phonon around $Q_0=(\frac{2}{3},\frac{2}{3},0)\pi/a$, which results in the premartensitic phase transition in β-phase NiTi, can be understood by the coupling of the phonons to the nested electronic states on the Fermi surface. The nesting plus strong e-ph interactions are the source of the phonon anomaly and the soft phonon. The coupling to the nested Fermi surface is quite sensitive to the temperature because thermal disorder and/or changes in the Fermi distribution reduce the effectiveness of the nesting at high temperature. The temperature dependence of the phonon anomaly can be explained as a smearing effect of the Fermi surface in the region of nesting.

ACKNOWLEDGMENTS

We would like to thank Dr. M. Keil, Dr. M. Müllner, and Dr. W. Weber, who were independently pursuing similar studies, and who joined us in the final stages of the work which resulted in the publication of Ref. 24. Their support has been much appreciated. Ames Laboratory is operated for the U.S. Department of Energy by Iowa State University under Contract No. W-7405-82. This work was supported by the Director for Energy Research, Office of Basic Energy Sciences of the U.S. Department of Energy.

[1]*Shape Memory Effects in Alloys,* edited by J. Perkins (Plenum, New York, 1975).

[2]H. C. Ling and R. Kaplow, Metall. Trans. A **12**, 2101 (1981).

[3]H. C. Ling and R. Kaplow, Mater. Sci. Eng. **51**, 193 (1981).

[4]K. Otsuka, T. Sawamutr, and K. Shimizu, Phys. Status Solidi A **5**, 457 (1971).

[5]G. D. Sandrock, A. J. Perkins, and R. F. Hehemann, Metal. Trans. **2**, 2769 (1971).

[6]L. Delaey, M. Chandrasekaran, M. Andrade, and J. Van Humbeeck, in *Proceedings of the International Conference on Solid-Solid Phase Transformations,* edited by H. I. Aaronson, D. E. Laughlin, R. F. Sekerka, and C. M. Wayman (Metallurgical Society of the AIME, New York, 1981), p. 1429.

[7]Many other references may be found in V. G. Pushin, V. V. Komdrat'ev, and V. N. Khachin, Izv. Vyssh. Uchebn. Zaved. Fiz. **5**, 5 (1985) [Sov. Phys. J. **28**, 341 (1985)].

[8]S. M. Shapiro, Y. Noda, Y. Fujii, and Y. Yamada, Phys. Rev. B **30**, 4314 (1984).

[9]K. Chandra and G. R. Purdy, J. Appl. Phys. **39**, 2176 (1968).

[10]S. K. Satija and S. M. Shapiro, Phys. Rev. B **29**, 6031 (1984).

[11]G. Herget, M. Müllner, G. Eckold, and H. Jex, in *Phonons 89,* edited by S. Hunklinger, W. Ludwig, and G. Weiss (World Scientific, Singapore, 1990), Vol. 1, p. 55.

[12]P. Moine, J. Allain, and B. Renker, J. Phys. F **14**, 2517 (1984).

[13]H. Tietz, M. Müllner, and B. Renker, J. Phys. C **17**, L529 (1984).

[14]M. Müllner, G. Herget, M. Keil, G. Eckold, J. B. Suck, and W. Weber, in *The Martensitic Transformation in Science and Technology,* edited by E. Hornbogen and N. Jost (DGM Informationsgesellschaft, Oberursel, 1989), p. 115.

[15]G. Herget, M. Müllner, J. B. Suck, R. Schmidt, and H. Wipf, Europhys. Lett. **10**, 49 (1989).

[16]H Tietze, M. Müllner, and P. Selgert, J. Phys. D **17**, 1391 (1984).

[17]O. Mercier, K. N. Melton, G. Gremaud, and J. Hagi, J. Appl. Phys. **51**, 1833 (1980).

[18]W. Buhrer, R. Gotthardt, A. Kulik, O. Mercier, and F. Staub, J. Phys. F **13**, L77 (1983).

[19]H. Tietze, M. Müllner, P. Selgert, and W. Assmus, J. Phys. F **15**, 263 (1985).

[20]I. Folkins and M. B. Walker, Phys. Rev. B **40**, 255 (1989).

[21]D. A. Papaconstantopoulos, G. N. Kamm, and P. N. Poulopoulos, Solid State Commun. **41**, 93 (1982).

[22]R. Bruinsma, Phys. Rev. B **25**, 2951 (1982).

[23]J. A. Krumhansl, in *Nonlinearity on Condensed Matter,* edited by A. R. Bishop, D. K. Campbell, P. Kumar, and S. E. Trullinger (Springer-Verlag, Berlin, 1986), p. 255.

[24]G. L. Zhao, T. C. Leung, B. N. Harmon, M. Keil, M. Müllner, and W. Weber, Phys. Rev. B **40**, 7999 (1989).

[25]J. A. Appelbaum and D. R. Hamann, in *Transition Metals,* edited by M. J. G. Lee, J. M. Perz, and E. Fawcett, IOP Conf. Proc. No. 39 (Institute of Physics, Bristol, 1977), p. 111; P. J. Feibelmann, J. A. Appelbaum, and D. R. Hamann, Phys. Rev. B **20**, 1433 (1979).

[26]J. C. Slater and G. F. Koster, Phys. Rev. **B 94**, 1498 (1954).

[27]C. M. Varma and W. Weber, Phys. Rev. Lett. **39**, 1094 (1977); Phys. Rev. B **19**, 6142 (1979); W. Weber, in *Electronic Structure of Complex Systems,* Vol. 113 of *NATO Advanced Study Institute, Series B: Physics,* edited by P. Phariseau and W. Temmerman (Plenum, New York, 1984).

[28]J. Rath and A. J. Freeman, Phys. Rev. B **11**, 2109 (1975).

[29]See Ref. 13 and G. Herget, Doctoral thesis, Johann Wolfgang Goethe Universitat, 1990.

[30]See Fig. 3 of Ref. 24.